Journal of Rock Mechanics and Geotechnical Engineering xxx (xxxx) xxx

Contents lists available at ScienceDirect

Journal of Rock Mechanics and Geotechnical Engineering

journal homepage: www.jrmge.cn

Full Length Article

Comprehensive analysis of multiple machine learning techniques for rock slope failure prediction

Arsalan Mahmoodzadeh [a,*], Abed Alanazi [b], Adil Hussein Mohammed [c], Hawkar Hashim Ibrahim [d], Abdullah Alqahtani [e], Shtwai Alsubai [b], Ahmed Babeker Elhag [f]

[a] Department of Civil Engineering, University of Halabja, Halabja, Kurdistan Region, 46018, Iraq
[b] Department of Computer Science, College of Computer Engineering and Sciences in Al-Kharj, Prince Sattam bin Abdulaziz University, P.O. Box 151, Al-Kharj, 11942, Saudi Arabia
[c] Department of Communication and Computer Engineering, Faculty of Engineering, Cihan University-Erbil, Kurdistan Region, Iraq
[d] Department of Civil Engineering, College of Engineering, Salahaddin University-Erbil, 44002, Erbil, Kurdistan Region, Iraq
[e] Software Engineering Department, College of Computer Engineering and Sciences, Prince Sattam bin Abdulaziz University, P.O. Box 151, Al-Kharj, 11942, Saudi Arabia
[f] Department of Civil Engineering, College of Engineering, King Khalid University, Abha, 61413, Saudi Arabia

ARTICLE INFO

Article history:
Received 24 May 2023
Received in revised form
28 July 2023
Accepted 14 August 2023
Available online xxx

Keywords:
Rock slope stability
Open-pit mines
Machine learning (ML)
Limit equilibrium method (LEM)

ABSTRACT

In this study, twelve machine learning (ML) techniques are used to accurately estimate the safety factor of rock slopes (*SFRS*). The dataset used for developing these models consists of 344 rock slopes from various open-pit mines around Iran, evenly distributed between the training (80%) and testing (20%) datasets. The models are evaluated for accuracy using Janbu's limit equilibrium method (LEM) and commercial tool GeoStudio methods. Statistical assessment metrics show that the random forest model is the most accurate in estimating the *SFRS* ($MSE = 0.0182$, $R^2 = 0.8319$) and shows high agreement with the results from the LEM method. The results from the long-short-term memory (LSTM) model are the least accurate ($MSE = 0.037$, $R^2 = 0.6618$) of all the models tested. However, only the null space support vector regression (NuSVR) model performs accurately compared to the practice mode by altering the value of one parameter while maintaining the other parameters constant. It is suggested that this model would be the best one to use to calculate the *SFRS*. A graphical user interface for the proposed models is developed to further assist in the calculation of the *SFRS* for engineering difficulties. In this study, we attempt to bridge the gap between modern slope stability evaluation techniques and more conventional analysis methods.

1. Introduction

Fracture mechanics has remained a prominent concern in the fields of academia and industry for decades. It involves the profound study of crack initiation, crack propagation, and their profound effects on the failure and deformation of structures. The stress intensity factor serves as a pivotal metric for pinpointing the crack tip, the precise location where stress reaches its zenith and the crack initiates its propagation. The discernment of fracture mechanics-related attributes pertaining to diverse materials assumes paramount importance in engineering designs. Consequently, the field of fracture mechanics, encompassing various materials, is advancing at an accelerated pace. In this context, slope stability emerges as one of the essential topics within the field of large-scale fracture mechanics. Hence, this article endeavors to delve into the analysis of slope stability by employing cutting-edge computational methods to calculate their safety factors.

The slope stability is a vital representation of rock, soil, or a mixed mass in the event of a variety of failures that result in the downstream movement of removable masses. Ground deformation at various scales caused by slope collapses is a major source of damage to buildings, roads, railroads, and infrastructure (Bromhead, 1992; Akgün and Koçkar, 2004). Slope mass shape, strain-stress history, geo-material conditions, external load conditions, the climate of the region, seismic activity, geo-structures, and

* Corresponding author.
E-mail address: arsalan.mahmoodzadeh@uoh.edu.iq (A. Mahmoodzadeh).
Peer review under responsibility of Institute of Rock and Soil Mechanics, Chinese Academy of Sciences.

https://doi.org/10.1016/j.jrmge.2023.08.023

pore water pressure conditions are all possible causes of instabilities. Sliding mass behavior and the possible slip surface expansion on slopes are analyzed about these triggering elements (Abramson et al., 2001). Failure, sliding, and overturning of slope masses may be facilitated by the specific geometry of the slopes involved. The higher the slope, the greater the risk of slipping (Akgün and Koçkar, 2004). Creep and plastic slips are time-dependent behaviors of loose soils that may be triggered by a slope's strain-stress history. One of the well-known characteristics that could provide a good condition for the slope instability is the geo-material state. Organic soils, loose layers, glacial deposits, and marl are universally considered as crucial factors in slope collapses (Huang, 2014). Seismic activities and external loadings may cause the slope to break under dynamic circumstances. Weathering refers to the gradual changes in slope conditions that may be attributed to regional climate.

Slope sliding is frequently triggered by weathering, which reduces the shear strength of soil grains. It is generally recognized that pore water pressure is a driving force in the collapse of slopes. The pore water pressure is one of the key factors in most stability analysis equations (Huang, 2014). The presence of groundwater in the soil and rocks, exerting pressure on the pores between particles, leads to increased fluidization and reduced interparticle friction within the soil (Abramson et al., 2001). In conclusion, folding, faults, and other complicated geological deformations are most frequently associated with geostructures. Common types of failures that may occur in these settings include debris, slope-toe erosion, and side-base instability. Many of these collapses occur on rock faces, while others have been seen on earth faces (Rotigliano et al., 2019; Bordoni et al., 2021).

By calculating the safety factor index, one may determine the slip surface, which acts as the key line between unstable and stable masses (Nanehkaran et al., 2023). Instabilities may be categorized as either earth slope failures or rock slope failures based on the underlying geology of the slope. Slopes on Earth behave like homogenous masses, which causes rotating (or huge failure) and planar shapes to be created. Slope conditions in rock are more nuanced and may be broken down into planar, toppling, wedge, and rotating failures. Slopes' safety factor may be calculated using the probable slippery mass situation, regardless of the sort of failure that happens on the slope. The safety factor may be approximated in two- and three-dimensions under dynamic and/or static circumstances by completing the vectors or moments of the polyhedral forces at the imagined sliding surface (Abramson et al., 2001). The slope mass will be in equilibrium, and the stability analysis will be sound if all the necessary conditions are satisfied, including the closure of these polyhedral force vectors. Not meeting several necessary conditions is a good example of non-closure polyhedral vectors (moments and/or forces) (Ullah et al., 2020).

On earth slopes, the sliding surface traverses the areas with the lowest resistance, and the safety factor is at a minimum when there are no resistant surfaces, no layers, and no bedrock with high strength. Hence, if the minimum safety factor is greater than the critical state (safety factor = 1), the slope will be steady. Conversely, the slope is unsteady if the minimum safety factor is less than the critical condition. Stabilizations based on an accurate estimate of the safety factor value enable dependable stability analysis of slopes. In the last three decades, engineers have created a variety of stability analysis techniques to assess the factor of safety and identify factors such as the probable slip surface, failure mechanism, and instability scale. These techniques can be categorized as limit state criteria, routine evaluations, limit equilibrium, hybrid, planar failure, high-order, numeric, and intelligent approaches (Chen et al., 2003; Azarafza et al., 2020). The limit equilibrium methods (LEMs) have garnered more attention than the others because they can be used with relative ease, require fewer assumptions, and can be generalized and inoculated against flaws in other techniques. In the field of stability research, various methods were explored in ancient times. However, it was Fellenius (1936) who paved the way for applying engineering and computational techniques to stability analysis. Fellenius method has stood the test of time and is widely recognized. It involves assessing stability by considering the equilibrium moment around the center of the failure circle, specifically on a circular slip surface. To quantify the magnitude of rotational failures, another influential figure in this field, Bishop (1955) presented a technique based on vertical force equilibrium and moment equilibrium. For the more difficult case of widespread failures, Nonveiller (1965) adapted Bishop's approach. Janbu et al. (1956) provided LEMs-based techniques for determining the stability conditions of earth slopes that may be used in the general form of slip surfaces. After these developments, researchers working on stability techniques using LEMs received much attention, which ultimately led to the development and widespread use of several different LEMs for use in stability analysis. The USACE, Swedish, Lowe-Karafiath, Morgenstern, Sarma, Spencer, and Correia approaches are only a few of the well-known ones that may be cited (Nanehkaran et al., 2023). In most cases, the estimated values for the safety factor are within 6% of one another, demonstrating that LEMs produce accurate results when computing the safety factor (Nanehkaran et al., 2023). As stated by Janbu et al. (1956), the LEM-based approaches may be universally applied to any slip surface and any failure mechanism. Because of the restrictions of the assumed surface for slip parameter assessments, the typical LEMs technique executes the progressive instability analysis using iterative procedures. The old techniques in LEM analysis, which are covered by the advancement of computer applications in slope stability analysis, have been greatly enhanced and are now capable of solving more intricate equations related to the safety factor. In particular, failure mechanism, the slope condition, and slide risk potential may all be predicted with great accuracy using computational intelligence approaches (Zhu et al., 2003; Li and Yang, 2019; Mathe and Ferentinou, 2021; Ahangari et al., 2022).

Machine learning (ML) techniques are relatively recent approaches to solving technical and scientific challenges. These methods have shown potential ability in estimating and predicting most engineering problems. Slope stability analysis utilizing predictive models has greatly benefited from the use of cutting-edge technology like artificial intelligence (AI) and, in particular, ML. With the use of ML and a focus on precision, predictive models aim to make predictions about and assessments of the safety factor. Algorithms for ML try to figure out how to learn from previous examples of data, or training data, and then apply that knowledge to new situations. Both deep learning and shallow algorithms are used in ML, with both types of algorithms aiming to make decision or prediction. The accuracy of predictions is directly influenced by the learning rate of algorithms, which corresponds to learning paradigms such as unsupervised, supervised, or reinforcement learning. No matter what kind of learning is used in the predictions, the efficacy of each algorithm may be evaluated.

Many motives may be used to categorize the major principles behind applying ML methods to generating a safety factor for slopes:

(1) The safety factor is an important parameter in the safety design. It is directly connected to the degree to which innovation and dependability are required to prevent slope failure. Consequently, it is vital to provide a safety factor with a low error rate and great accuracy. The error rate of computations is higher when using conventional methods, which

are mostly based on simplified assessments and specific assumptions.
(2) Uncertainties in the assessment procedure frequently limit the accuracy of estimates in slope stability analysis. The ability to account for such ambiguities is frequently beyond the scope of more conventional approaches. Yet, because of the repetition involved in the learning process, ML can cover these uncertainties laterally, enhancing performance.
(3) The accuracy and performance of learning models during prediction operations are evaluated using essential pillars of ML analysis, i.e. confusion matrix, error table, or loss function. These powerful tools allow for precise measurement and assessment of the effectiveness of learning models. Standard techniques of stability analysis lack this capacity. Evaluating the reliability of the model is important for making decisions and implementing the best stabilizing techniques. As a result, stabilizing tactics are decided upon in conventional approaches based on experience (Nanehkaran et al., 2023).

Because of the inherent uncertainty in geotechnical engineering applications, ML approaches may be successfully utilized to construct robust prediction models for slope stability as well as to anticipate and stabilize important parameters. Most empirical and statistical evaluations fail to account for uncertainty, which increases the error rate in stability analysis. The evaluation of slope safety coefficient for various indicators is challenged by the unpredictability of factors such as pore water pressure, slope geometry, geo-material characteristics, and slope strength qualities. These elements pose significant challenges due to their inherent variability and make accurate assessment a formidable task. Methods that are more capable and efficient than the uncertainties being faced are thus prioritized. The ML processes are powerful instruments for accomplishing this aim (Abramson et al., 2001).

The current research made an effort, using several widely used ML methods, to produce accurate models for estimating the safety factor of rock slopes (*SFRS*). Long-short-term memory (LSTM), support vector regression (SVR), gradient boosting regression (GBR), null space SVR (NuSVR), Gaussian process regression (GPR), K-nearest neighbors (KNN), extreme gradient boosting (XGBoost), random forests (RF), extra tree regression (ETR), hist-gradient boosting regression (HGBR), voting regression (VR), and decision tree regression (DTR) were all examined as potential main analytic cores. Due to their remarkable attributes and numerous advantages, these algorithms have garnered widespread adoption among academics, particularly in the domains of geotechnical analysis and domain stability. Here is a concise overview of their notable benefits:

(1) They possess the capability to process both nonlinear and linear data for regression and classification purposes.
(2) Employing decision boundaries in the form of hyper-planes, nodes, or neurons, they effectively distinguish between different groups.
(3) By carefully considering options and weighing costs and potential advantages, they facilitate the calculation of capabilities and errors.
(4) These algorithms significantly reduce computation time and offer the potential for utilization across all stages of assessment and stabilization, with the accuracy of calculations being adaptable to the complexity of the study.
(5) They enable more precise estimations, leading to a reduction in errors.
(6) Their simplicity and effectiveness make them highly accessible and efficient tools.

The presentation of such models has the potential to diminish prevailing uncertainties surrounding slope stability, catalyzing for the advancement of ML methods in the field. By showcasing these models, we can establish a solid foundation upon which further developments can be made, revolutionizing the way we approach slope analysis and ensuring enhanced safety standards. A block diagram of the proposed research is shown in Fig. 1 step by step.

The contributions of this work include:

(1) Investigating a variety of rock slopes in different open-pit mines in Iran to obtain more comprehensive data.
(2) Investigating the performance of 12 ML methods to predict the *SFRS*.
(3) Fine-tuning the hyperparameters of each model to achieve the most robust estimations.
(4) Comparison of the models' behaviors with practice.
(5) Parameters' sensitivity analysis.
(6) Providing a graphical user interface (GUI) based on the ML models for the *SFRS* estimation.

2. Machine learning methods

LSTM is an artificial neural network used in DL and AI. LSTM, a powerful neural network, diverges from the conventional feedforward networks by integrating feedback connections. Not only can this kind of recurrent neural network (RNN) analyze individual data points, but it can also process whole sequences of data. Because of this, LSTM networks are effective in data processing and prediction (Hochreiter and Schmidhuber, 1997). ETR harnesses the collective power of multiple random decision trees fitted to diverse subsets of the dataset, exerting concerted efforts to enhance prediction accuracy while mitigating the risks of overfitting. This ingenious approach amalgamates the outcomes of these individual trees, culminating in a formidable final model that surpasses the capabilities of its constituent components (Friedman, 2001; Piryonesi and El-Diraby, 2020). This approach belongs to the class of learning algorithms, and it has repeatedly shown the efficiency of a simple or basic algorithm. This conclusion, however, is sensitive to the characteristics of the supplied data (Hastie et al., 2009; Piryonesi and El-Diraby, 2020).

Harnessing Gradient Boosting Regression (HGBR) offers an ingenious solution for discretizing continuous variables, thereby expediting the tree-learning process. This groundbreaking technique paves the way for accelerated computations, significantly enhancing efficiency and performance. XGBoost, a dominant player in Gradient Boosting Regression (GBR), emerges as an unparalleled force. Built upon decision trees, XGBoost stands as the epitome of power and sophistication in GBR. When it comes to deriving the final output value, XGBoost employs a probability threshold of 0.5, deftly crafting an estimate that encapsulates the essence of the data (Dehestani et al., 2022).

The SVR technique, introduced by Cortes and Vapnik (Cortes and Vapnik, 1995), employs quadratic programming to select the optimal line after linear classification of a dataset. When it comes to regression problems, SVR becomes the go-to technique, while the NuSVR is a variant of SVR, and it incorporates the concept of "nu" parameter to control the number of support vectors and errors tolerated during the training process. GPR, taking a Bayesian and nonparametric approach to regression, has been causing quite a stir in the ML community. GPR's ability to give uncertainty measures for predictions and its strong performance on tiny datasets are two of its most appealing features (Rasmussen, 2004).

The DTR method, on the other hand, constructs regression trees by breaking down a dataset into smaller and smaller subsets,

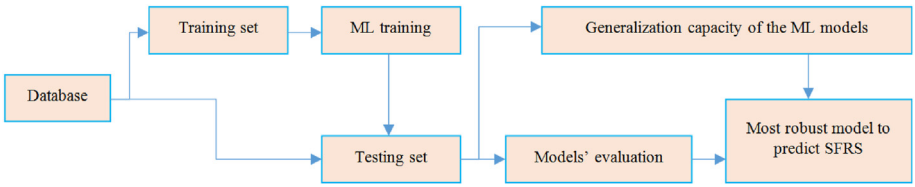

Fig. 1. Block diagram of this work.

ultimately generating a decision tree where nodes represent choices and leaves represent outcomes (Quinlan, 1986). RF, a powerful ensemble learning method, can be applied to many problems including classification and regression. During training, RF generates numerous decision trees, and the final prediction for regression tasks is the average of all the individual tree predictions (Ho, 1998).

VR, a subset of ensemble meta-estimators, utilizes multiple base regressions to accurately estimate the parameters of interest. By averaging several separate projections, VR arrives at the final prediction (Erdebilli and Devrim-İçtenbaş, 2022). In the KNN algorithm, if two points are significantly distant from each other, this information can be leveraged to make determinations. Each piece of information is weighted according to how well it matches the training data (Cover and Hart, 1967).

3. Modeling procedure

3.1. Dataset preparation

To put the standard-setting learning algorithms to work, a large main dataset was used. The primary dataset consists of 344 observations of rock slope stability obtained from several open-pit mines in Iran. Specifically, the aforementioned dataset was split into two parts: A training set (consisting of 80% of the data) and a testing set (consisting of 20% of the data). To enhance the effectiveness and versatility of the forecasting models, we would eagerly incorporate additional datasets with broader ranges. By augmenting the volume of data and expanding the parameters' scope, we can amplify the flexibility and applicability of these models. For instance, if we aspire to employ the prediction models outlined in this study to forecast the *SFRS* for a new slope, it is imperative that the input parameters of the new slope fall within the ranges covered by the training datasets of these models. Deviating from these established ranges would inevitably compromise the accuracy and reliability of the prediction models, rendering their outcomes less dependable. Therefore, a meticulous alignment between the input parameter ranges and the models' training datasets is paramount to achieve the desired precision in *SFRS* prediction.

Making a reliable prediction is of paramount importance. Thus, verifying the validity of the database should be a top priority. Realistically, a reliable database needs not just reliable data but also a sizable amount of data encompassing the whole range of parameter values for the factors that affect the issue being examined. One approach to reducing the dimensionality of data is to build a model using just a subset of the observable characteristics (predictor variables). Models for a subset are frequently chosen by picking the ones with the least expected error. Predictor subsets may be found with the use of algorithms, which are limited in their scope by parameters such as the number of characteristics to be considered and the number of features to be disregarded. In scenarios where preserving the original units and significance of features is paramount, and the objective is to unearth a compelling subset, feature selection reigns supreme over feature modification. Feature selection is optimal for decreasing dimensionality when only category features are available.

This article focuses on reducing the complexity of data by employing the stepwise technique. Stepwise regression, a method of sequentially selecting features, is utilized specifically for least-squares fitting. In this method, we consider the features that have the lowest p-values. To determine which predictor has the lowest p-value, the stepwise regression method first fits the model with each predictor separately. Next, choose that variable and use it, together with the one we picked in the previous step, to fit the model, while eliminating the others one by one. Once again, we go with the hypothesis with the lowest p-value. It is important to remember that the newly added variable should not dilute the significance of the previously chosen variable. In this study, we repeated this process until we found a set of variables where the p-value was less than 0.05.

An analysis of the results from the stepwise technique revealed that six factors, including slope angle (α), slope height (H), pore pressure ratio (r_u), cohesion (c), friction angle (φ), and unit weight (γ), have the largest impact on the *SFRS*. Therefore, this study employs a database with six-dimensional input training vectors (1×6). Parameter *SFRS* is also included in the one-dimensional (1×1) training vector output. Fig. 2 vividly illustrates the intricate interplay between a slope's geometry and the pivotal parameters that profoundly influence its stability. It is imperative to acknowledge that this study, while comprehensive in its scope, has deliberately excluded the consideration of external factors that may trigger slope failures, such as the seismic impact of earthquakes or other anthropogenic influences. The 80% of datasets (279 datasets) were used for training. The remaining 80% were used in test cases, totaling 65 datasets. Table 1 summarizes the datasets that may be accessed. The median, interquartile range, lowest, maximum, and first, second, and third quartiles are shown for each metric in this table.

The violin plot combines the information offered in a box plot with a kernel density plot. The goal is to improve people's ability to understand and value data that is expressed numerically. Violin plots can show both summary statistics and the density of each variable, while box plots are restricted in this regard. The distribution of the data may be shown by plotting estimates of the kernel density on each side of the graph. The likelihood that members of the population will have a particular value rises as one moves from

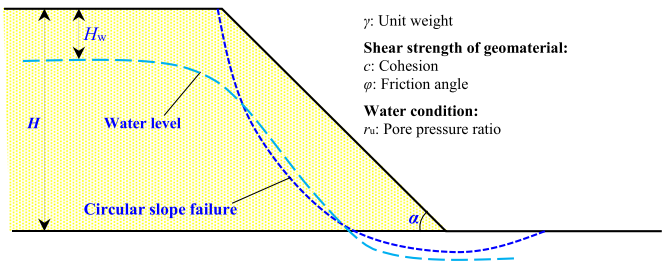

Fig. 2. A slope geometry and the parameters effective on its stability.

Table 1
An overview of the datasets applied in this study.

Dataset	Characterization	γ (kN/m^3)	c (kPa)	φ (°)	α (°)	H (m)	r_u	*SFRS*
Training set	Count	279	279	279	279	279	279	279
	Mean	20.46	15.58	27.38	34.51	61.29	0.19	1.26
	Standard deviation	3.76	14.99	10.48	10.3	69.02	0.17	0.38
	Minimum	14	0	0	16	3.6	0	0.24
	25%	18.5	3.65	21	27	10	0	1.02
	50%	20	11.71	30	34	31	0.25	1.2
	75%	22.4	24	35	45	88	0.3	1.45
	Maximum	28.44	55	45	65	219	0.64	2.31
Testing set	Count	65	65	65	65	65	65	65
	Mean	22.1	21.37	29.26	37.92	84.12	0.16	1.25
	Standard deviation	3.7	17.96	10.07	11.33	74.97	0.18	0.33
	Minimum	14	0	0	20	3.66	0	0.65
	25%	20	8.62	24	30	12.8	0	1.03
	50%	22	16.28	32	40	50	0	1.22
	75%	25	35	35	45	135	0.25	1.44
	Maximum	28.44	56	45	60	216	0.5	2.05

the more open sections of the violin plot to the more closed ones. Parameters are shown graphically in Fig. 3 as violin plots.

At the initial stage of this investigation, descriptive statistics were run on the primary datasets. Fig. 4 shows boxplots for all of the parameters. At a glance, we can observe that the datasets are non-symmetrical since the median line is not located in the middle of the box for all parameters. Another critical issue that must be accounted for in data processing is the presence of outlier values for a parameter. Outliers make it more difficult to identify patterns in data collection. Our ability to create reliable forecasting models is enhanced by the removal of anomalous information such as outliers and clusters. As can be observed in Fig. 4, there are no extreme values for any of the parameters.

A principal component analysis (PCA) of the dataset is described below. The multivariate statistical technique of principal component analysis may be used to investigate discrepancies and identify trends. Moreover, this method might be used to reduce the number of dimensions in difficult issues (the number of independent variables). In the PCA, the principal components (PCs), which are linear combinations of the original variables, are used to best explain the differences across datasets. Table 2 displays the coefficients (eigenvalues) and percentage of variation of the PCs. To determine which PCs best describe the variability in a dataset, scree charts may be quite helpful (see Fig. 5). The top two PCs explain 74% of the total variance in the data, as seen by the scree plot. Fig. 6 displays

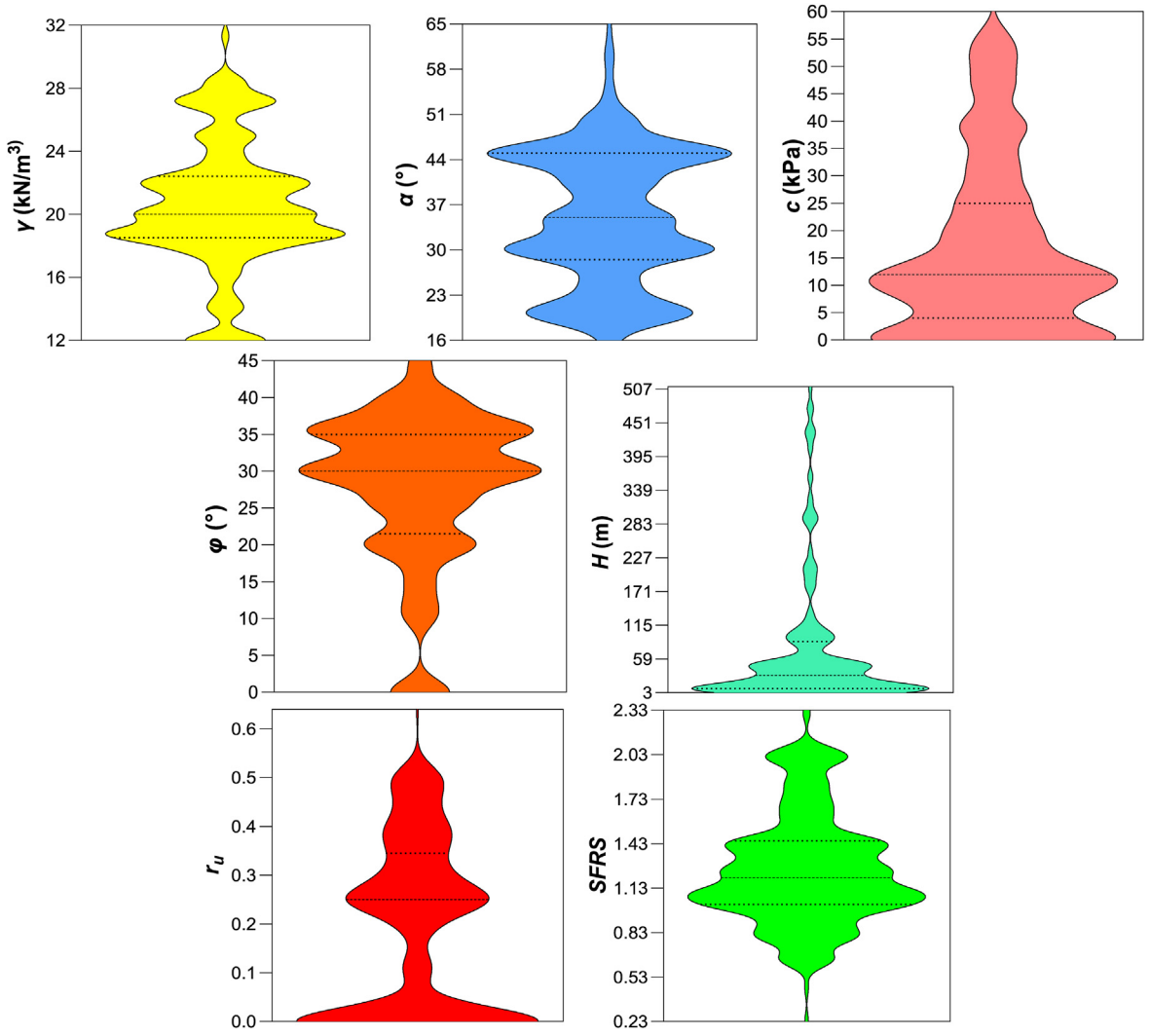

Fig. 3. The violin diagrams for the parameters.

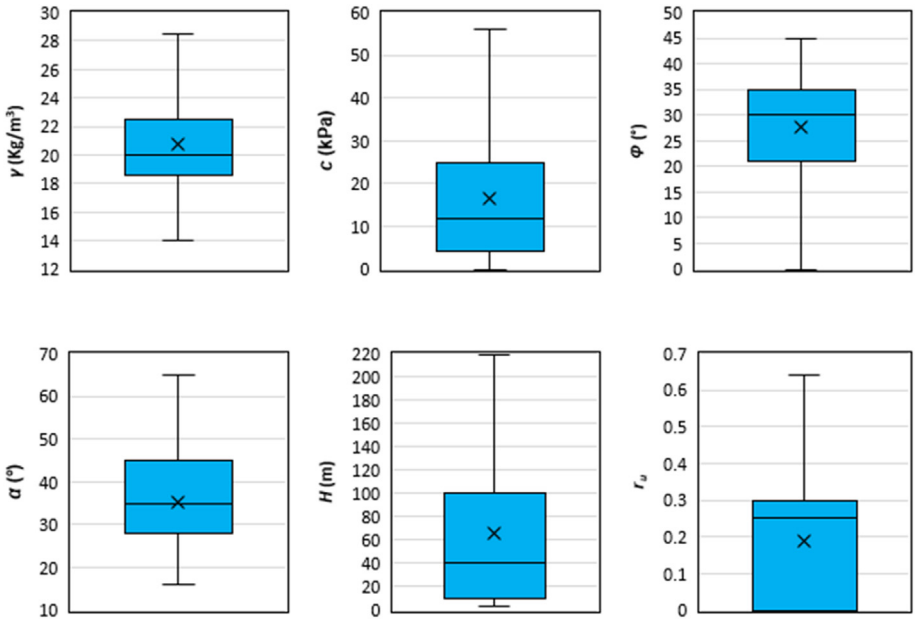

Fig. 4. Dataset's boxplots.

Table 2
Coefficients for the PCs.

Variable	Principal component						
	PC1	PC2	PC3	PC4	PC5	PC6	PC7
γ	−0.507	−0.106	0.135	0.344	0.264	0.712	0.136
c	−0.429	−0.239	−0.219	0.112	−0.746	−0.144	0.349
φ	−0.404	0.342	0.466	−0.314	0.23	−0.35	0.478
α	−0.375	0.495	−0.164	−0.455	−0.249	0.247	−0.508
H	−0.476	−0.085	−0.326	0.336	0.377	−0.521	−0.366
r_u	0.082	0.464	0.462	0.634	−0.319	−0.106	−0.222
SFRS	−0.15	−0.589	0.608	−0.221	−0.126	−0.074	−0.437
Eigenvalue	2.537	1.32	1.087	0.968	0.67	0.296	0.123
Variability (%)	39.247	34.855	10.525	6.827	4.572	2.223	1.75
Cumulative proportion (%)	39	74	85	91	96	98	100

the scatter plot for the first two PCs. The dataset does not have a clear natural grouping and is an outlier for this measure.

3.2. Implementation of the models

To execute the ML models, we harnessed the power of the Jupyter Notebook environment provided by Anaconda Navigator version 3.7. Anaconda, a remarkable program for scientific computing in Python, offers not only a cost-free solution but also streamlines package management and execution processes. The calculations were performed on a high-performance Intel (R) Core (TM) i7-10750H CPU running at an impressive 2.6 GHz, accompanied by a substantial 32 GB RAM capacity. This formidable hardware setup ensured optimal computational capabilities, enabling us to tackle complex tasks with efficiency and precision.

All the ML models were optimized based on the training datasets to show the highest performance in the *SFRS* estimation. To optimize each of the models, the type or value of their hyperparameters must be set to an optimal state. In this study, the trial-and-error method was used to fine-tune the models' hyperparameters. The practice of trial and error is routinely used to find answers to difficult questions. The agent will exhaust all possible avenues of attack before giving up or achieving success. There will be many attempts at solving this problem before the optimal one is found. Each ML method's adjusted hyperparameters and parameters are listed in Table 3.

3.3. Models validation

The utilization of mathematical models is indispensable in unraveling, simulating, and predicting intricate environmental phenomena and systems. Irrespective of the application domain, the evaluation of these forecasting outcomes is imperative. In all evaluations, the forecasts are rigorously scrutinized against pertinent observations through a range of statistical measures, commonly known as indices. These indices serve as powerful tools, shedding light on various facets of the disparities between the forecasted values and the actual measurements of the parameters. By comprehensively assessing these differences, we gain a comprehensive understanding of the model's performance and its alignment with real-world observations.

In this article, to evaluate the potential of the ML models in the prediction of *SFRS*, their results were compared with the results estimated using the LEMs and GeoStudio commercial software through five statistical evaluation metrics including the coefficient of determination (R^2), the mean absolute error (*MAE*), the mean squared error (*MSE*), the mean absolute percentage error (*MAPE*), and the *a*10_*index* (Eqs. (1)–(5)).

$$R^2 = 1 - \frac{sum\ squared\ regression}{sum\ of\ squares\ total} \tag{1}$$

$$MAE = \left(\frac{1}{n}\right)\sum_{i=1}^{n}|M_i - F_i| \tag{2}$$

$$MSE = \left(\frac{1}{n}\right)\sum_{i=1}^{n}(M_i - F_i)^2 \tag{3}$$

$$MAPE = \frac{100\%}{n}\sum_{i=1}^{n}\left|\frac{M_i - F_i}{M_i}\right| \tag{4}$$

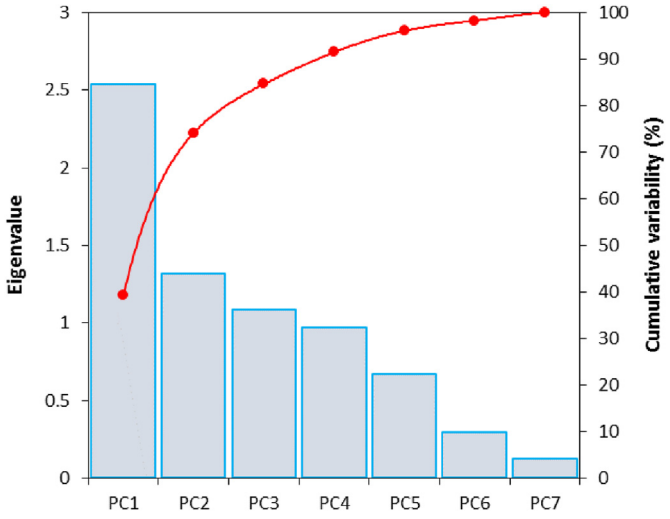

Fig. 5. Scree plot for the first seven PCs.

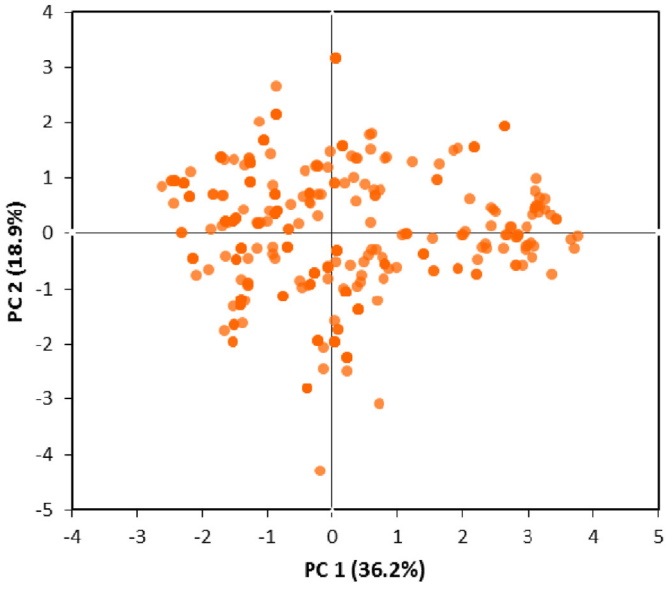

Fig. 6. Scatter plot of the PC1 against the PC2.

$$a10\_index = \frac{m10}{n} \tag{5}$$

where F_i and M_i denote the forecasted and measured values, respectively; n is the number of samples; and $m10$ is the number of samples having *experimental/forecasted* ratios between 0.9 and 1.1.

4. Results and discussion

We can evaluate the effectiveness of each ML model now that it has been fine-tuned on the training datasets. These quantitative metrics may be used as yardsticks to compare different ML models' efficacy. The comparison between the results estimated by each of the ML models and the results obtained from the LEM method is presented in Fig. 7 through the *a*10_*index* metric. As can be seen, all the models have provided high accuracy in the estimation of the *SFRS*. Thus, the lowest accuracy is obtained by the LSTM model (*a*10_*index* = 0.7077). Also, the highest accuracy is provided by the RF model (*a*10_*index* = 0.9077). Other models have provided accuracies between these two models.

Table 3
Optimized parameters and hyper-parameters of the ML algorithms.

Method	Parameters/Hyper-parameters
DTR	criterion = mse random state = 3
KNN	Number of neighbors = 1
SVR	kernel = *RBF* C = 4 epsilon = 0.05
GPR	seed = 0 random state = 0 kernel = Constant Kernel (constant−value = 1, constant−value−bounds = (0, 0.08)) * *RBF* (length−scale = 0.5, length−scale−bounds = (0, 10)) + *RBF* (length−scale = 2, length−scale−bounds = (0, 10))
LSTM	number of hidden layers = 4 number of genes for each hidden layer = 32 kernel initializer = lecun uniform activation function = ReLU Loss = mse Bach size = 8 Epochs = 100
XGBoost	cv = 5 verbose = 1
RF	Number of iterations = 200 cv = 2, verbose = 1 random state = 38
ETR	Number of estimators = 10 Random state = 0
HGBR	Maximum depth = 200 learning rate = 0.07 loss = mse
GBR	Number of estimators = 1000 Maximum depth = 4 Minimum samples split = 5 Learning rate = 0.02 loss = 'ls'
NuSVR	C = 5 Cache size = 200 gamma = 'scale' kernel = RBF maximum iterations = -1 nu = 0.5
VR	Number of estimators = 6 Random state = 2 lr = 'drop'

mse: mean squared error; RBF: Radial basis function; nu: null space.

We employ a variety of other statistical measures (R^2, *MSE*, *MAPE*, and *MAE*) to assess ML models' efficacy in addition to the *a*10_*index*. The statistical metrics for each model are shown in Table 4. Numerous statistical metrics are used to assess the models' performance. Finally, the votes are in, and each model has been ranked. Table 4 displays the rankings numerically. Fig. 8 is a visual representation of the information in Table 4. These results suggest that the RF model is more accurate than its LSTM counterpart. The following ranking was generated based on the prediction accuracy of each model: RF → DRT → XGBoost → HGBR → (GBR, ETR) → GPR → SVR → KNN → NuSVR → VR → LSTM.

So far, we have created several ML models that estimate the *SFRS* with impressive predictive precision. Therefore, it is advisable to investigate input trends and *SFRS* output patterns to guarantee generalization capacities rather than only looking at the cross-correlation (Mahmoodzadeh et al., 2023). To do this, we keep certain inputs constant while varying others within a range (Mahmoodzadeh et al., 2021). To begin, we want to evaluate the models' efficacy by varying one input parameter, H, over its range of values (4–214 m), while keeping all other inputs fixed (γ = 20 kN/m^3, c = 15 kPa, φ = 27°, α = 34°, r_u = 0.2). In reality, the *SFRS* decreases when H is increased, creating more favorable circumstances for slope collapse. Using the ML models, we now look at how the *SFRS* shifts as a function of the parameter H. For each of the trained ML models, Fig. 9 displays how the *SFRS* varies concerning the parameter H. All ML models exhibit a declining trend in the *SFRS* as a function of increasing the parameter H. The SVR and NuSVR models are the only ones that consistently predict a declining *SFRS*. The *SFRS* has varied across other ML models when the parameter H has been increased, sometimes becoming larger, shrinking, and staying the same. Therefore, only the SVR and NuSVR models have shown themselves to be accurate in this scenario.

By varying c between 0 kPa and 55 kPa and holding all other settings constant (H = 60 m, γ = 20 kN/m, φ = 27°, α = 34°, r_u = 0.2), we can see how the ML models affect the resulting *SFRS* results. The *SFRS* is known to rise as a function of the parameter c in practice. Fig. 10 shows how the *SFRS* changes compared to the parameter c for each of the trained ML models. The only model that always shows an increasing trend for the *SFRS* is the NuSVR model. The *SFRS* has varied across other ML models when c has been

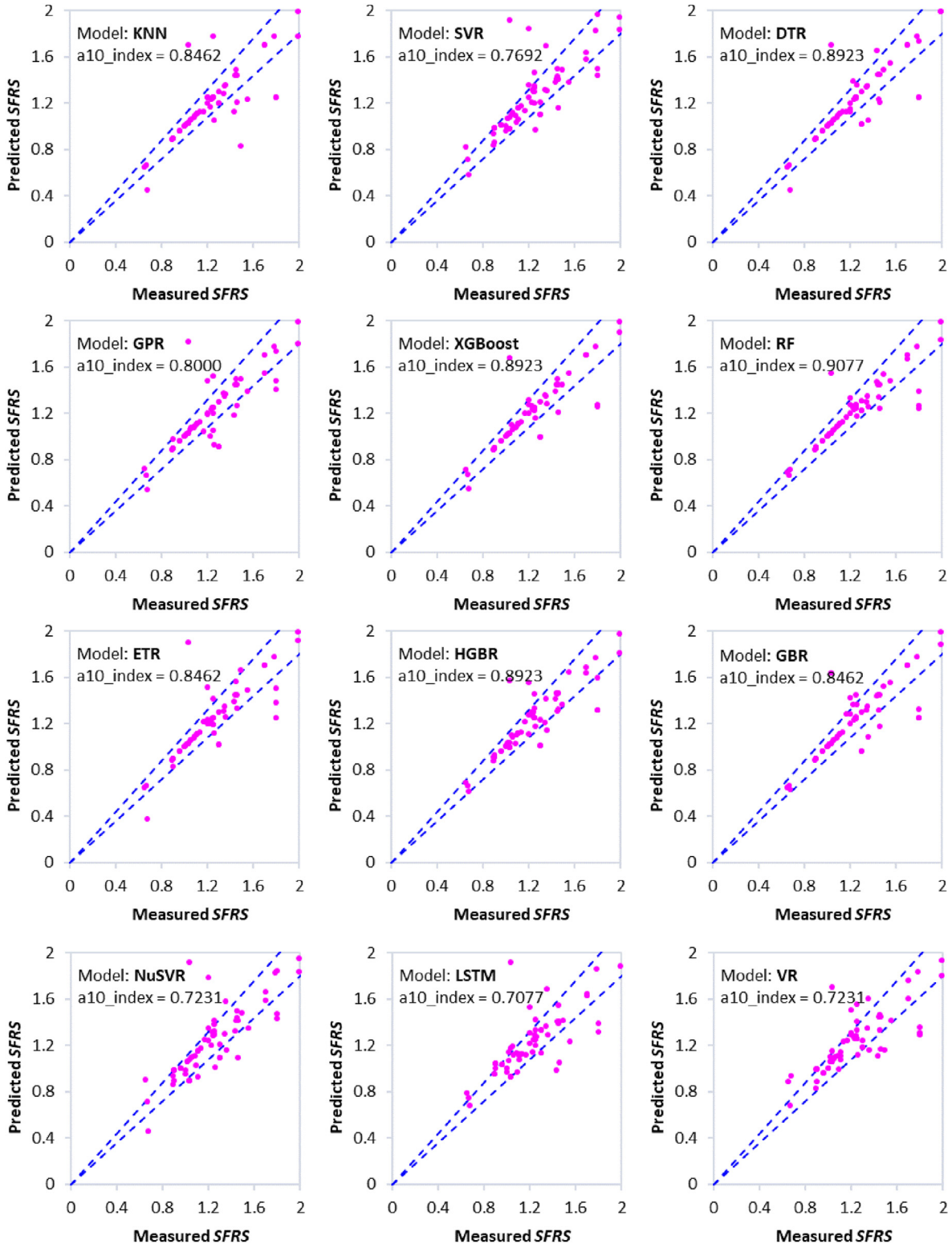

Fig. 7. Comparison of the ML and LEM results.

Table 4
Performance assessment of the ML models for the *SFRS* estimation through scoring the statistical index results.

Model	*MSE*	Score	R^2	Score	*MAE*	Score	*MAPE*	Score	*a10_index*	Score	Rank
KNN	0.0378	1	0.6501	1	0.084	5	0.061	5	0.8462	5	17
SVR	0.033	6	0.6946	5	0.11	4	0.091	3	0.7692	3	21
DTR	0.0241	10	0.7766	10	0.063	11	0.048	8	0.8923	6	45
GPR	0.0271	8	0.7491	7	0.08	7	0.063	4	0.8	4	30
XGBoost	0.0245	9	0.7731	9	0.064	10	0.048	8	0.8923	6	42
RF	0.0182	12	0.8319	12	0.054	12	0.038	9	0.9077	7	52
ETR	0.0278	7	0.7427	6	0.071	9	0.057	6	0.8462	5	33
HGBR	0.0211	11	0.805	11	0.081	6	0.061	5	0.8923	6	39
GBR	0.0269	5	0.7509	8	0.072	8	0.052	7	0.8462	5	33
NuSVR	0.0339	4	0.6861	4	0.118	3	0.1	1	0.7231	2	14
LSTM	0.037	2	0.6618	2	0.121	2	0.098	2	0.7077	1	9
VR	0.034	3	0.6856	3	0.122	1	0.098	2	0.7231	2	11

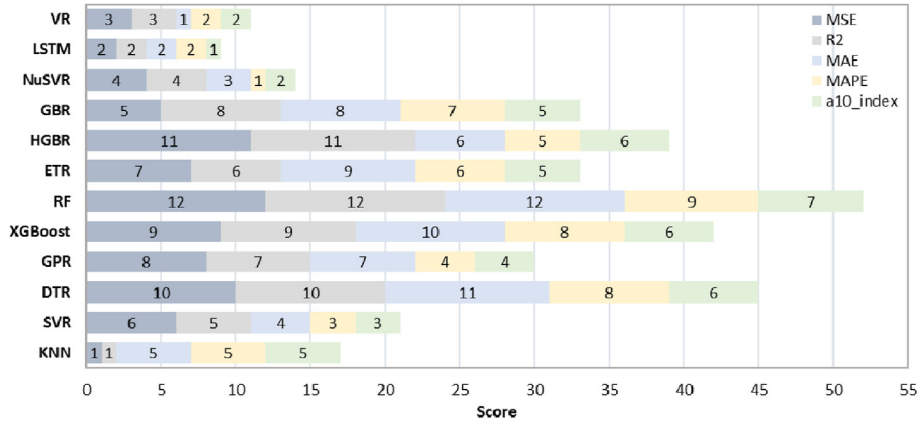

Fig. 8. Ranking score of the ML models for the *SFRS* estimation.

increased, sometimes going up, going down, and staying the same. Therefore, only the NuSVR model, out of all the ML models used in this research, has shown accurate behavior when compared to the actual mode.

Now we want to examine the performance of the NuSVR model more about the practice mode. For this purpose, we simultaneously change the parameters r_u and α within their ranges and keep the other parameters constant ($H = 60$ m, $\gamma = 20$ kN/m^3, $\varphi = 27°$, $c = 15$ kPa). In practice, by increasing the parameter α and decreasing the parameter r_u, the *SFRS* decreases. According to Fig. 11, the NuSVR model exhibits an identical behavior to the practical mode. Therefore, this study presents the NuSVR model as a model with a high potential for estimating the *SFRS*.

It is important to note that ML models can only be developed and presented when the necessary training data are available. Otherwise, alternative techniques, e.g. numerical simulations, may need to be employed. As we continue to enter the era of data, efforts are being made to enhance ML models for predicting *SFRS* by harnessing more comprehensive and powerful datasets. While various studies have been conducted on the predictive capabilities of ML methods for *SFRS*, it is crucial to address the limitations of these models. Most studies focus on specific conditions, resulting in models that lack comprehensiveness. Therefore, instead of completely changing the model types used in previous studies, it is more beneficial to enrich the existing databases. This approach would enable the development of a versatile model capable of accurately estimating the safety factor for a wide range of slopes. Presenting a model that can only predict the safety factor for a specific slope limits its practicality. There is still much work to be done to create a model that can effectively capture the safety factor of the majority of slopes under diverse conditions. Constructing such an ML-based model requires a comprehensive database, which necessitates collaboration among researchers worldwide.

5. Sensitivity analysis

To provide context for the results, we may do a sensitivity analysis to see which model parameters were most influential. A solid understanding of this topic is crucial for reducing data dimensionality and avoiding model overfitting. In this research, the mutual information (MI) technique was used for the sensitivity analysis.

MI is a feature selection method that borrows the concept of information gain from information theory and applies it to practical problems like building decision trees. The MI between two variables measures the amount we can infer about one variable from observations of the other. Implementing MI is a breeze when dealing with categorical input and output data. It was originally designed to deal with textual data. Nevertheless, it may be adapted to handle numerical data as well. MI's success may be measured by how much entropy it has managed to eliminate. Take Eq. (6) as an example. The MI score must be an integer more than zero and less than or equal to infinity. A high MI value indicates that the feature is important for training the model and so should be given more weight in the final score. However, if the MI score is low, for example 0, then there is little to no correlation between the trait and the goal.

$$MI(feature; target) = Entropy(feature) - Entropy(feature|target) \quad (6)$$

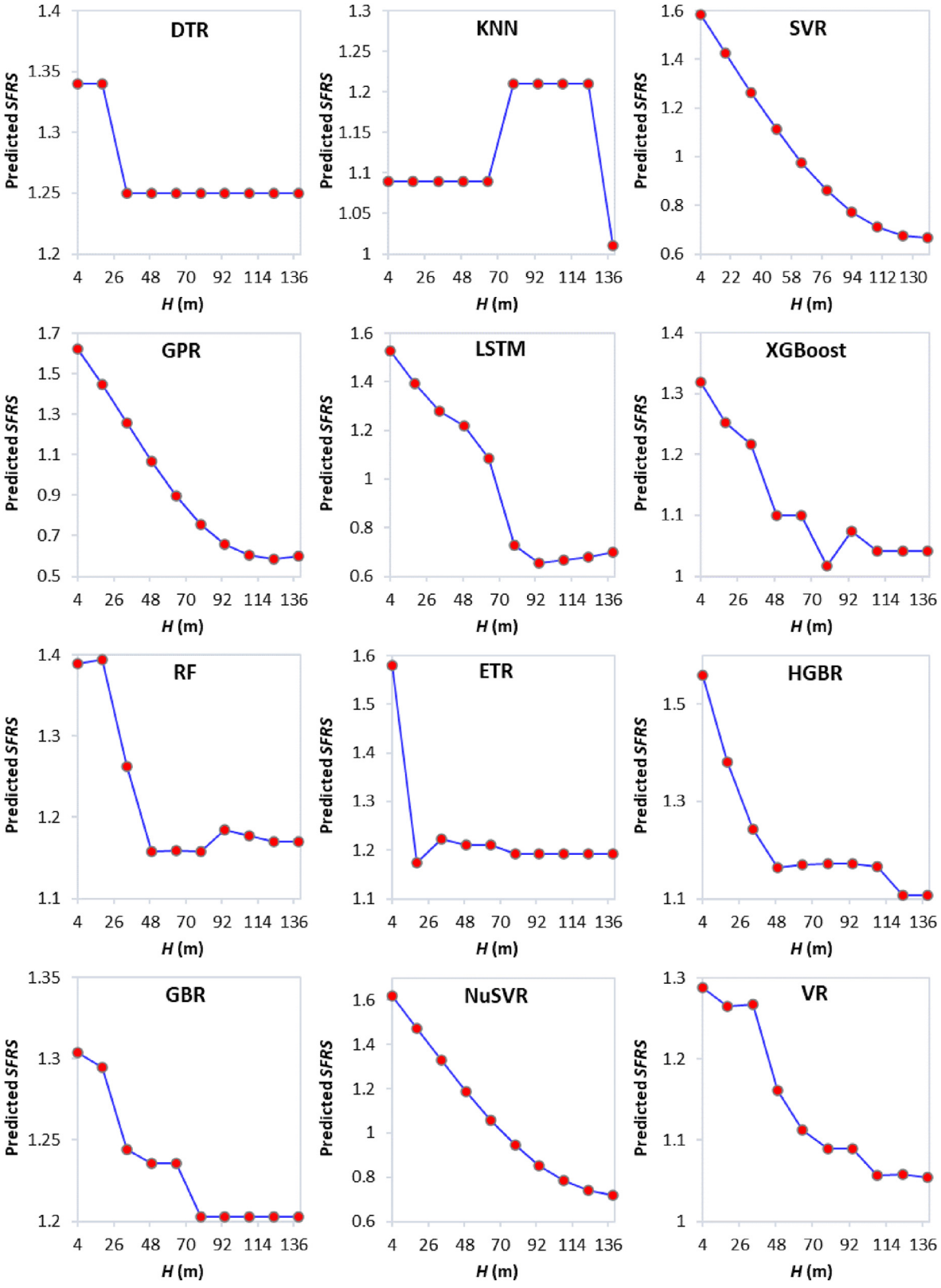

Fig. 9. Behavior of the ML models about the parameter *H* (all other inputs are held constant).

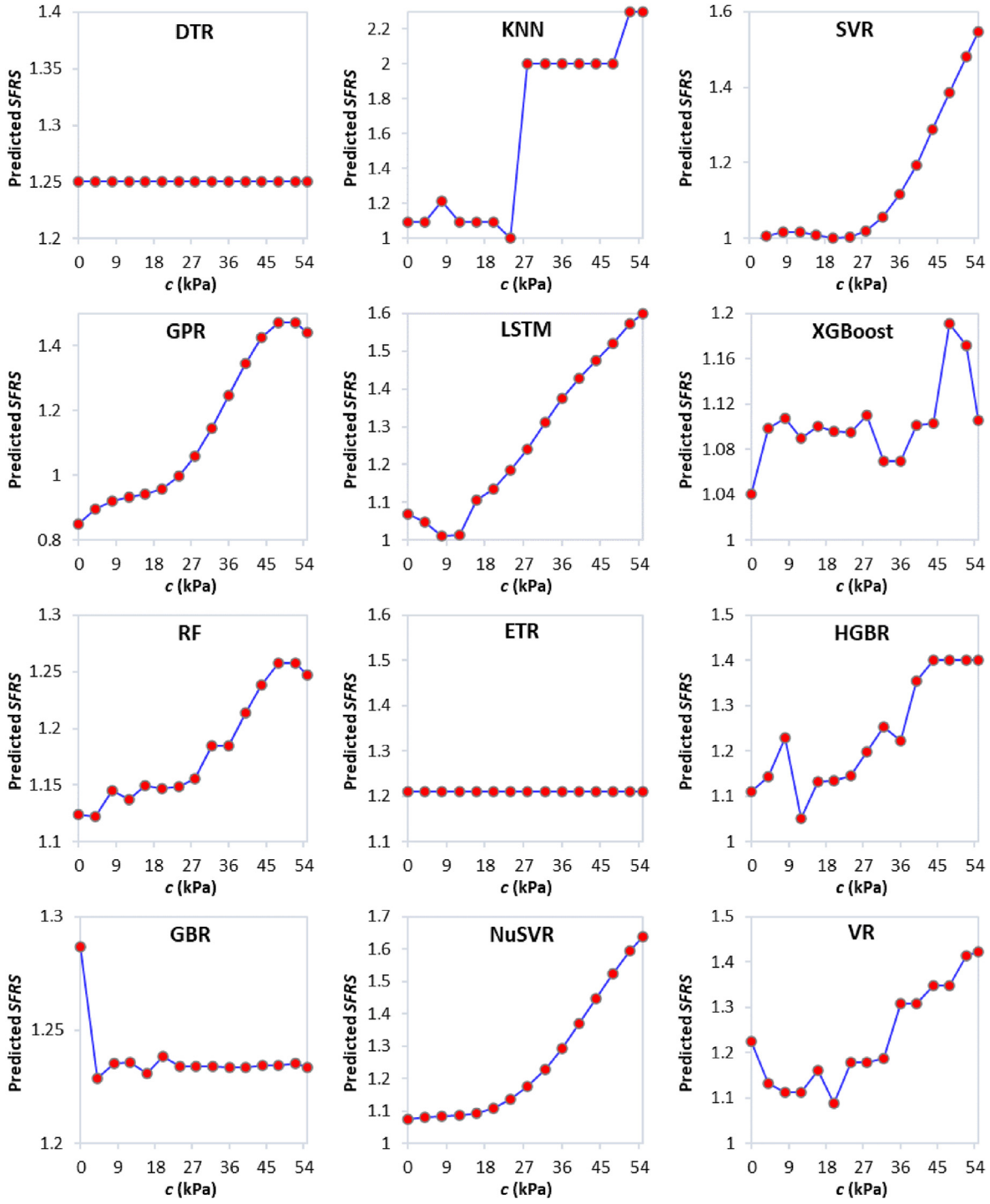

Fig. 10. Behavior of the ML models about the parameter *c* (all other inputs are held constant).

The estimated MI scores for all of the inputs are shown in Fig. 12. It is clear that the γ and r_u parameters are linked to the best and worst impacts. The effect of other parameters on the *SFRS* is also significant.

6. Graphical user interface

GUIs are user-friendly tools that offer ML-based prediction models for estimating the *SFRS*. The software encompasses a comprehensive set of twelve ML algorithms. As the prediction models are initially trained on experimental data points, there is no requirement to retrain them for *SFRS* estimation. The GUI is thoughtfully designed and easy to navigate (see Fig. 13). Once the user inputs the necessary parameters into the GUI, the trained ML algorithms can accurately estimate the *SFRS*. Compared to alternative methods, the GUI provides fast and cost-effective *SFRS* estimation with high accuracy. Furthermore, it serves as a valuable platform for researchers interested in compiling datasets related to the *SFRS*. The computation time for each ML model ranges from as little as 2 s to a maximum of 157 s.

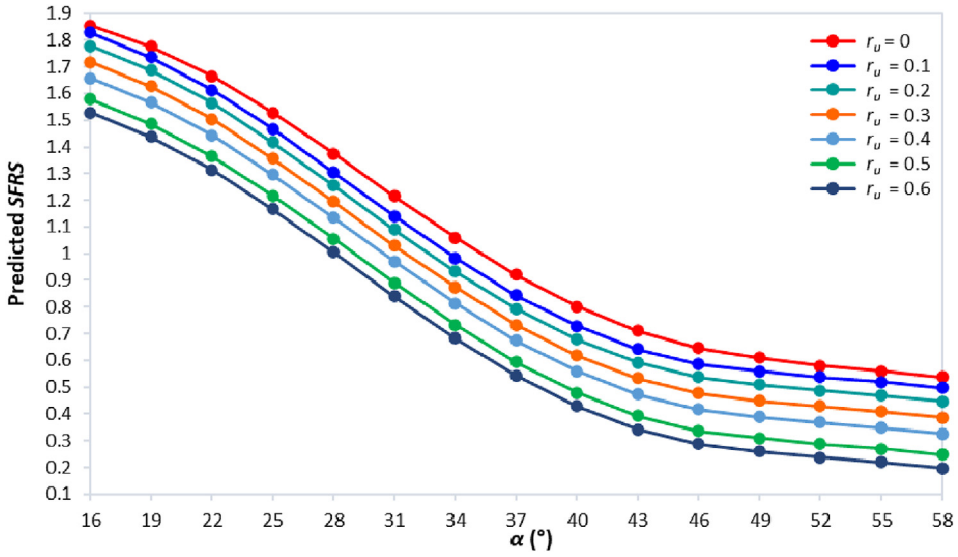

Fig. 11. The *SFRS* vs. the parameters α and r_u for the NuSVR model (all other inputs are held constant).

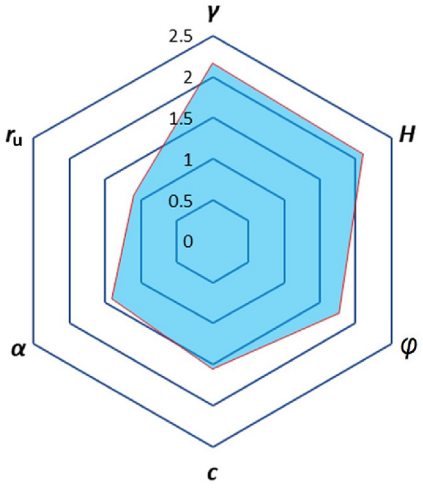

Fig. 12. Parameters' sensitivity score.

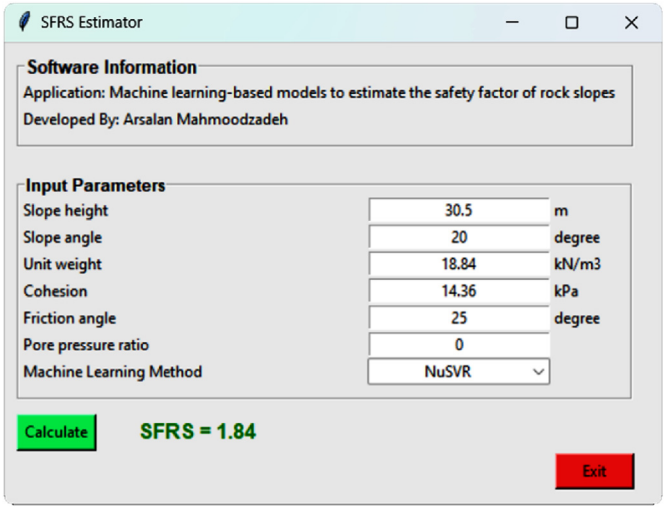

Fig. 13. The developed GUI.

7. Conclusions

The following conclusions can be drawn from this study:

(1) A step-by-step examination of the data revealed that the *SFRS* is significantly impacted by the parameters *H*, *c*, r_u, α, γ, and φ.
(2) ML-based models can be a practical replacement for other costly and time-consuming methods for determining the *SFRS*.
(3) The prediction accuracy of the models was ranked according to a comparison of their results with those of the LEM: RF → DRT → XGBoost → HGBR → (GBR, ETR) → GPR → SVR → KNN → NuSVR → VR → LSTM
(4) The NuSVR model was recommended for the *SFRS* estimation because its performance was found to be more accurate than that of the other models when comparing the behavior of the ML models with the practice mode.
(5) The sensitivity analysis results revealed that the γ and r_u parameters are linked to the best and worst impacts on the *SFRS*, respectively. The effect of other parameters on the *SFRS* was also significant.
(6) To enhance the estimation of the *SFRS* for engineering challenges, a cutting-edge GUI software for the ML-based models was meticulously developed.
(7) In this study, an effort was made to bridge the gap between modern slope stability evaluation techniques and more conventional methods of analysis. This study holds significant importance as it empowers geotechnical engineers with the capability to accurately estimate the *SFRS* without the need for extensive time and financial resources.

Forecasting the *SFRS* is an arduous undertaking characterized by intricate uncertainties stemming from the interconnectedness of

numerous influencing variables. In the development of ML-based models for *SFRS* prediction, this investigation has focused solely on six interrelated parameters. However, it is imperative to acknowledge that future iterations of the dataset will incorporate more consequential factors, enhancing the comprehensiveness of the model. The pursuit of a more precise and robust intelligent *SFRS* forecasting model necessitates a vast and extensive database. To ensure the proposed model's efficacy in estimating *SFRS* for diverse slopes, its hyperparameters must be meticulously fine-tuned, aligning with the magnitude and intricacy of the dataset. This meticulous calibration guarantees optimal performance, empowering engineers with unprecedented accuracy and reliability in *SFRS* estimation. In addition, for future works, improving the performance accuracy of *SFRS* models using other metaheuristic optimization algorithms is also suggested.

Declaration of competing interest

The authors declare that they have no known competing financial interests or personal relationships that could have appeared to influence the work reported in this paper.

Acknowledgments

This study is supported via funding from Prince Satam bin Abdulaziz University project number (PSAU/2024/R/1445). The authors extend their appreciation to the Deanship of Scientific Research at King Khalid University for funding this work through large Group Research Project (Grant No. RGP. 2/357/44).

References

Abramson, L.W., Lee, T.S., Sharma, S., Boyce, G.M., 2001. In: Slope Stability and Stabilization Methods, second ed. Wiley-Interscience.

Ahangari, Y.N., Pusatli, T., Chengyong, J., Chen, J., Cemiloglu, A., Azarafza, M., Derakhshani, R., 2022. Application of machine learning techniques for the estimation of the safety factor in slope stability analysis. Water 14 (22), 3743.

Akgün, H., Koçkar, M.K., 2004. Design of anchorage and assessment of the stability of openings in silty, sandy limestone: a case study in Turkey. Int. J. Rock Mech. Min. Sci. 41 (1), 37–49.

Azarafza, M., Akgün, H., Feizi-Derakhshi, M.-R., Azarafza, M., Rahnamarad, J., Derakhshani, R., 2020. Discontinuous rock slope stability analysis under blocky structural sliding by fuzzy key-block analysis method. Heliyon 6 (5), e03907.

Bishop, A.W., 1955. The use of the slip circle in the stability analysis of slopes. Geotechnique 5 (1), 7–17.

Bordoni, M., Vivaldi, V., Lucchelli, L., Ciabatta, L., Brocca, L., Galve, J.P., Meisina, C., 2021. Development of a data-driven model for spatial and temporal shallow landslide probability of occurrence at catchment scale. Landslides 18 (4), 1209–1229.

Bromhead, E., 1992. In: The Stability of Slopes, second ed. Taylor & Francis.

Chen, Z., Mi, H., Zhang, F., Wang, X., 2003. A simplified method for 3D slope stability analysis. Can. Geotech. J. 40 (3), 675–683.

Cover, T., Hart, P., 1967. Nearest neighbor pattern classification. IEEE Transact. Inform. Theory 13 (1), 21–27. https://doi.org/10.1109/TIT.1967.1053964.

Dehestani, A., Kazemi, F., Abdi, R., Nitka, M., 2022. Prediction of fracture toughness in fibre-reinforced concrete, mortar, and rocks using various machine learning techniques. Eng. Fracture Mech. 276, 108914. https://doi.org/10.1016/j.engfracmech.2022.108914.

Erdebilli, B., Devrim-İçtenbaş, B., 2022. Ensemble voting regression based on machine learning for predicting medical waste: a case from Turkey. Mathematics 10 (14), 2466. https://doi.org/10.3390/math10142466.

Fellenius, W., 1936. Calculation of stability of earth dam. In: Proceedings of the 2nd Transaction Congress on Large Dams.

Friedman, J.H., 2001. Greedy function approximation: A gradient boosting machine. Ann. Stat. 29 (5). https://doi.org/10.1214/aos/1013203451.

Hastie, T., Tibshirani, R., Friedman, J., 2009. The Elements of Statistical Learning. Springer, New York. https://doi.org/10.1007/978-0-387-84858-7.

Ho, T.K., 1998. The random subspace method for constructing decision forests. IEEE Transactions on Pattern Analysis and Machine Intelligence 20 (8), 832–844. https://doi.org/10.1109/34.709601.

Hochreiter, S., Schmidhuber, J., 1997. Long Short-Term Memory. Neural Comput. 9 (8), 1735–1780. https://doi.org/10.1162/neco.1997.9.8.1735.

Huang, Y.H., 2014. Slope Stability Analysis by the Limit Equilibrium Method. American Society of Civil Engineers. https://doi.org/10.1061/9780784412886.

Janbu, N., Bjerrum, L., Kjaernsli, B., 1956. Soil Mechanics Applied to Some Engineering Problems. Norwegian Geotechnical Institute.

Li, Y.X., Yang, X.L., 2019. Soil-slope stability considering effect of soil-strength nonlinearity. Int. J. GeoMech. 19 (3). https://doi.org/10.1061/(ASCE)GM.1943-5622.0001355.

Mahmoodzadeh, A., Mohammadi, M., Hashim Ibrahim, H., Nariman Abdulhamid, S., Ghafoor Salim, S., Farid Hama Ali, H., Kamal Majeed, M., 2021. Artificial intelligence forecasting models of uniaxial compressive strength. Transport. Geotech. 27, 100499.

Mahmoodzadeh, A., Ghafourian, H., Hussein Mohammed, A., Rezaei, N., Hashim Ibrahim, H., Rashidi, S., 2023. Predicting tunnel water inflow using a machine learning-based solution to improve tunnel construction safety. Transport. Geotech. 40, 100978.

Mathe, L., Ferentinou, M., 2021. Rock slope stability analysis adopting Eurocode 7, a limit state design approach for an open pit. IOP Conf. Ser. Earth Environ. Sci. 833 (1), 012201.

Nanehkaran, Y.A., Licai, Z., Chengyong, J., Chen, J., Anwar, S., Azarafza, M., Derakhshani, R., 2023. Comparative analysis for slope stability by using machine learning methods. Appl. Sci. 13 (3), 1555.

Nonveiller, E., 1965. The Stability Analysis of Slopes with a Slip Surface of General Shape. 6th International Conference on Soil Mechanics and Foundation Engineering (Montréal).

Piryonesi, S.M., El-Diraby, T.E., 2020. Data analytics in asset management: cost-effective prediction of the pavement condition index. J. Infrastruct. Syst. 26 (1). https://doi.org/10.1061/(ASCE)IS.1943-555X.0000512.

Quinlan, J.R., 1986. Induction of decision trees. Mach. Learn. 1 (1), 81–106. https://doi.org/10.1007/BF00116251.

Rasmussen, C.E., 2004. Gaussian Processes in Machine Learning, pp. 63–71. https://doi.org/10.1007/978-3-540-28650-9_4.

Rotigliano, E., Martinello, C., Hernandéz, M.A., Agnesi, V., Conoscenti, C., 2019. Predicting the landslides triggered by the 2009 96E/Ida tropical storms in the Ilopango caldera area (El Salvador, CA): optimizing MARS-based model building and validation strategies. Environ. Earth Sci. 78 (6), 210.

Ullah, S., Khan, M.U., Rehman, G., 2020. A brief review of the slope stability analysis methods. Geol. Behav. 4 (2), 73–77.

Zhu, D.Y., Lee, C.F., Jiang, H.D., 2003. Generalised framework of limit equilibrium methods for slope stability analysis. Geotechnique 53 (4), 377–395.

Arsalan Mahmoodzadeh is a doctoral candidate specializing in rock mechanics within the Rock Mechanics Division at the School of Engineering, Tarbiat Modares University, Iran. Additionally, he holds a membership in the international research group at the University of Halabja, Iraq. Arsalan received his BSc degree from the University of Kordestan, Iran, and pursued his MSc degree at Shahrood University of Technology, Iran. His primary research interests revolve around the applications of machine learning and artificial intelligence in the domains of tunneling, rock mechanics, geotechnical engineering, and fracture mechanics. Arsalan has published over 60 research papers, showcasing his extensive contributions to these fields.